

# Nonsteroidal Anti-Inflammatory Drug Solid-State Microencapsulation on Green Activated Carbon – Mass Transfer and Host-Guest Interactions



This work is licensed under a Creative Commons Attribution 4.0 International License

Z. Lyubanova Yaneva\*

Chemistry Unit, Department of Pharmacology, Animal Physiology and Physiological Chemistry, Faculty of Veterinary Medicine, Trakia University, Students Campus, 6000 Stara Zagora, Bulgaria

<https://doi.org/10.15255/CABEQ.2019.1656>

Original scientific paper

Received: April 22, 2019

Accepted: July 10, 2019

The present study investigated the drug-carrier capacity of green activated carbon derived from fruit stones by steam-gas activation (ACSTA) towards the nonsteroidal anti-inflammatory drug (NSAID) ibuprofen (IBU), and assessed the host-guest interactions and mass transfer mechanism/s of the drug microencapsulation and *in vitro* release processes. The mass transfer studies outlined that the process of IBU encapsulation on ACSTA microparticles was predominantly controlled by intraparticle solid phase diffusion.

*Keywords:*

microencapsulation, ibuprofen, activated carbon, *in vitro* release

## Introduction

The development of innovative controlled-release (CRS) systems for biologically active substances, which are becoming increasingly widely used in medicine, pharmaceuticals and agriculture, is one of the top priority areas of scientific research in the field of medical chemistry over the last decade.<sup>1</sup>

Microencapsulation of pharmaceutically active substances into appropriate carrier matrices ensures sustained or prolonged release of the drug; protection and stabilization of moisture-, photo- and oxidation-sensitive biologically active compounds; prevention of incompatibility between drugs; predominant therapeutic action to specific activity sites.<sup>2</sup> Adsorption of drug molecules in porous micro-carrier particles is a readily adoptable microencapsulation technique for thermo-, photolabile drugs, and such, with limited solubility. The micro-, meso- and macro-porosity structure of the carriers is significant in providing sustained drug delivery.<sup>3</sup>

Drug delivery systems (DDS) are based on a variety of carriers, such as polymers, modified natural and synthetic mineral matrices, micro- and nanomaterials, etc., applied alone or in different combinations.<sup>3–5</sup> The main qualitative indicators for assessing the effectiveness of CRS are the degree of incorporation and subsequent *in vitro* controlled release of the biologically active substance, which depend on the physicochemical and mechanical

properties of the composite, on the molecular characteristics and properties of the organic substances, and on the interactions between the carrier and the incorporated substance.<sup>6</sup>

The efficiency of activated charcoal and its proven antitoxic activity due to its large specific surface area, high adsorption capacity and microporous structure provoked *in vitro* and *in vivo* studies on the potential of a variety of newly synthesized activated carbon based carriers as precursors for the development of effective DDS.<sup>7</sup> Studies have been carried out on the adsorption of amino acids, vitamins, enzymes, and proteins on mesoporous carriers based on silica and activated carbon. McCary and Rybolt investigated the incorporation of acetaminophen into various porous carbon-containing materials and subsequent release in phosphate buffer medium at a temperature of 37 °C and pH 7.0.<sup>8</sup> Contemporary research has shown that, in agriculture, newly developed controlled-release systems based on active carbon, unlike conventional forms, facilitate gradual and controlled release of pesticides, reduce evaporation losses and minimize soil and water pollution caused by organic priority pollutants.<sup>1,9</sup>

*In vitro* studies on adsorption of metoprolol, pindolol, salbutamol, furosemide and clonidine on activated carbon demonstrated that, although the drug affinity for the carrier is in good agreement with their hydrophobicity, the desorption rate is not proportional to their hydrophilicity, and was significantly influenced by the particle size.<sup>10</sup> Effective use of activated carbon as an oral adsorbent in the

\*Corresponding author: E-mail: z.yaneva@abv.bg; Tel.: +359 898 399 203

primary treatment of acute theophylline poisoning has been investigated *in vitro*. The amount of theophylline adsorbed by physiological saline was found to be greater than that of aqueous solution, and the increase in the contact area, by decreasing the particle size, increased the rate of adsorption.<sup>11</sup> The investigations of Tominaga *et al.* of a new treatment with activated charcoal swabs showed a remarkable improvement in the symptoms of bacterial vaginosis when treated with activated charcoal swabs.<sup>12</sup> This approach showed effective treatment of this infection without adverse side effects.

The comparative review and analysis of the recently published scientific results proves the applicability but also the existence of a number of disadvantages of universal and alternative activated carbons and mixtures of composites with carbon-containing materials as “carriers” of biologically active molecules, mainly in terms of controlling and achieving an optimal degree of desorption of the active ingredient in real or simulated biological medium.

Therefore, the outline of this new priority area in medical chemistry, and the lack of investigations on the applicability of innovative Bulgarian activated carbon derived from waste fruit stones as a carrier of biologically active substances, provoked the objectives of the current research. Detailed studies on the encapsulation of biologically active substances are significant and useful only if they include extensive study of the equilibrium, kinetics of encapsulation and release behavior, as well as the rate limiting mass transfer mechanism/s.<sup>13–15</sup>

The aim of the present study was to investigate the drug-carrier capacity of green activated carbon derived from fruit stones by steam-gas activation (ACSTA) towards the nonsteroidal anti-inflammatory drug (NSAID) ibuprofen, and to assess the host-guest interactions and mass transfer mechanism/s of the drug microencapsulation and *in vitro* release processes.

## Materials and methods

### Chemicals

Ibuprofen (C<sub>13</sub>H<sub>18</sub>O<sub>2</sub>, CAS No. 15687-27-1, HPLC, 99.9 %), NaCl (p.a., > 99.5 %), NaOH (p.a. > 98 %) and HCl (reagent grade, 37 %) were supplied by Sigma-Aldrich. The activated carbon derived from fruit stones by steam-gas activation (ACSTA) was supplied by “GANDEV-ELI-ILIA GANDEV” ET, Kamenovo Village, Bulgaria. Its physicochemical characteristics are presented in Table 1.

Table 1 – Physicochemical characteristics of ACSTA

Characteristic parameter	Value
Fractional composition, μm	250–500
Absorption activity towards I <sub>2</sub> , mg g <sup>-1</sup>	600
Absorption activity towards CH <sub>3</sub> COOH	580
Total ash, %	0.08
Specific surface area, m <sup>2</sup> g <sup>-1</sup>	490
pH	6.5–7.5
Moisture, %	2.5
Bulk density, g dm <sup>-3</sup>	630

### UV/Vis analyses

The drug concentrations in liquid and solid phase were determined by UV/VIS spectrophotometer DR 5000 Hach Lange (Germany), supplied with 10 mm quartz cuvettes. The absorbance spectra were measured at maximum wavelength  $\lambda = 263$  nm with 2 nm slit with 900 nm min<sup>-1</sup> scan speed and very high smoothing. All UV/Vis analyses were made in triplicate.

### Potentiometric titration, point of zero charge, and microscopic analyses

The determination of the acidic and basic active sites and functional groups on the AB surface was performed by potentiometric titration of 1.000 g of the solid phase with 0.1 M NaOH and 0.1 M HCl. The point of zero charge (pH<sub>PZC</sub>) of ACSTA was experimentally determined by the solid phase addition method.<sup>16</sup> The microscopic morphological analyses of the activated carbon were performed with a broadband digital binocular optical microscope 50–1000x (Biomed).

### FTIR spectroscopy

FTIR spectra of ACSTA and ibuprofen-loaded ACSTA were determined on Bruker Tensor 37 FTIR spectrometer using KBr pellet technique. For each sample, 64 scans were collected at a resolution of 2 cm<sup>-1</sup> over the 4000–400 cm<sup>-1</sup> wavenumber region.

### Solid-state drug microencapsulation

Ibuprofen solid-state encapsulation on ACSTA microparticles was accomplished by the addition of 0.050 g solid carrier to six IBU/EtOH solutions with initial concentrations in the range 25–200 μg mL<sup>-1</sup> and volume 20 mL each. The obtained experimental series was agitated for 100 h on IKA®KS 130 Basic Shaker at 560 rpm, pH 7.0, and temperature 25 °C. The solid dispersion systems were filtered through 0.45 μm sterile syringe filters (Sartorius Minisart®)

and centrifuged at 8000xg on Heraeus Labofuge 200 (Thermo, Electron Corporation) centrifuge. The NSAID concentrations in the supernatants were measured spectrophotometrically. The encapsulation efficiency of IBU into the ACSTA support was calculated by:

$$E, \% = \frac{(\text{total amount of drug} - \text{amount of free drug})}{\text{total amount of drug}} \cdot 100 \quad (1)$$

The parameter drug loading capacity (DLC) expresses the amount of drug in the particles divided by the weight of the carrier system. DLC was calculated by:

$$\text{DLC, \%} = \frac{(\text{total amount of drug} - \text{amount of free drug})}{\text{microparticles weight}} \cdot 100 \quad (2)$$

The time dependence of the microencapsulation process was investigated in a standard batch reactor with a Heidolph impeller. In 60-mL IBU/EtOH solution with initial concentration 100  $\mu\text{g mL}^{-1}$  were added 0.400 g ACSTA. The system was subjected to constant mixing at 450 rpm, at  $T = 25\text{ }^\circ\text{C}$  for 180 min. Samples (3.5 mL) from the bulk system, taken at definite time intervals, were filtered through 0.45  $\mu\text{m}$  sterile syringe filters (Sartorius Minisart®) and centrifuged at 8000xg on Heraeus Labofuge 200 (Thermo, Electron Corporation) centrifuge. The NSAID concentrations in the supernatants were measured spectrophotometrically.

### **In vitro release study**

*In vitro* IBU release behavior in simulated biological medium was investigated by agitating 0.300 g dried NSAID-loaded ACSTA composite samples dispersed in 20 mL simulated gastric fluid solution (without pepsin) – 0.2 % (w/v) NaCl in 0.7 % (v/v) HCl, at pH 1.2, and at constant temperature  $T = 37 \pm 0.5\text{ }^\circ\text{C}$  in a Digital Waterbath WNB 22 (Memmert GmbH). The kinetics *in vitro* release experiments were conducted in standard batch mode equipment consisting of a vessel (25 mL) and a Heidolph impeller at constant agitation rate 100 rpm. With respect to the constructive dimensions, the following ratios and correlations are valid:

$$z = D; b = 0.5 \cdot D; h = 1/3 \cdot z,$$

where  $z$  is the solution height (m);  $D$  – vessel diameter (m);  $b$  – paddle blades height (m);  $h$  – distance between the vessel bottom and the paddle bottom (m).

At various time points, supernatants were isolated by centrifugation, and 3.5 mL sample was taken out instead of the same volume of fresh medium. The amount of released drug was analyzed spectrophotometrically at 263 nm.

### **Interpretative modelling**

The experimental equilibrium isotherms were described by five mathematical equilibrium models (Table 4). The kinetics experimental data of IBU microencapsulation on ACSTA particles was analyzed by assessment of the applicability of six kinetics, mass transfer and diffusion mathematical models (Table 5). The mathematical models applied to the experimental data of IBU release from the obtained drug-delivery composite are listed in Table 7.

### **Error functions analyses**

The experimental data was analyzed by linear and non-linear regression analyses and determination of the corresponding correlation coefficients ( $R^2$ ) and SSE, MSE, RMSE and chi-square ( $\chi^2$ ) error functions.

## **Results and discussion**

### **UV/VIS absorption spectra of IBU**

The absorption spectra of IBU in the UV region were registered at the specific wavelength  $\lambda = 263\text{ nm}$  (Fig. 1a) for all tested drug initial concentrations and contained no additional interference peaks that could influence the analytical results. The standard plot of IBU characterized with high correlation coefficient ( $R^2 = 0.995$ ) (Fig. 1b).

### **Surface characterization of ACSTA**

The importance of the surface characteristics of the carrier in driving and modulating the biochemical fate of organic molecules is now a solid and well-assessed key fact. The physicochemical properties of organic surfaces play a crucial role in determining the interaction of a solid with bio-active organic molecules.<sup>17</sup>

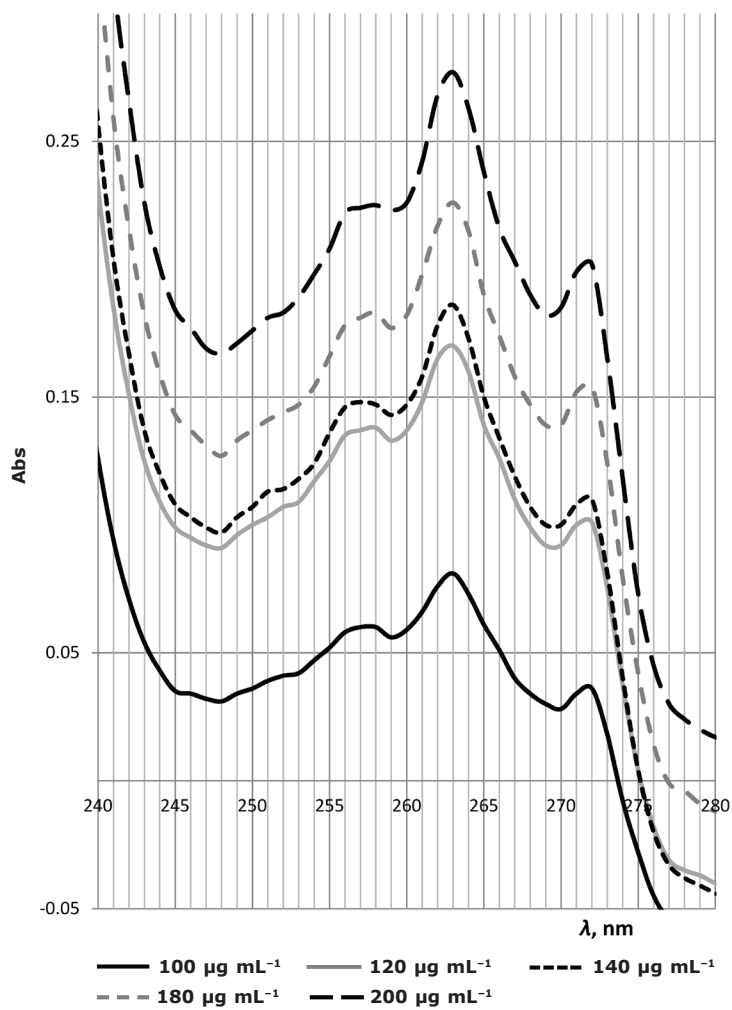
### **Digital microscopy**

The digital microscopic images of ACSTA at 10x, 100x, 400x and 1000x magnification (Fig. 2) display the high porosity of the microparticles and the homogeneous nature of the solid surface.

### **Point of zero charge**

Point of zero charge is of fundamental importance in surface science. In the field of drug-delivery systems design, it determines how easily a carrier is able to adsorb biologically active molecules. The  $\text{pH}_{\text{pZC}}$  of ACSTA was determined to be 9.6. Consequently, at pH 7.0, i.e., below  $\text{pH}_{\text{pZC}}$ , the activated carbon surface is positively charged.

(a)



(b)

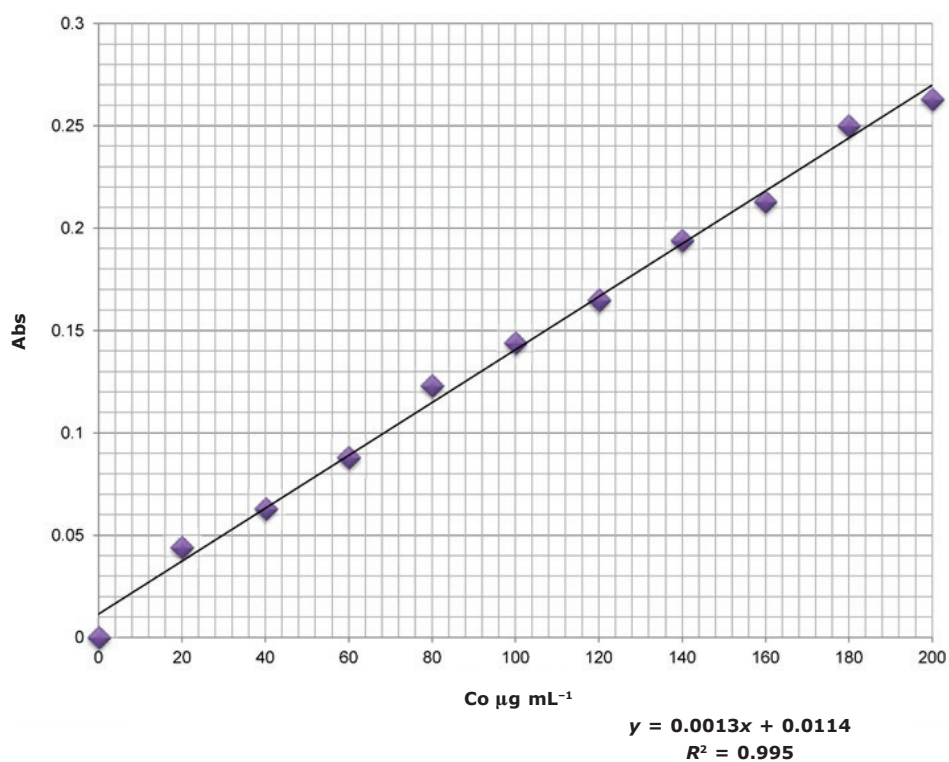


Fig. 1 – a) UV absorption spectra and b) calibration curve of ibuprofen

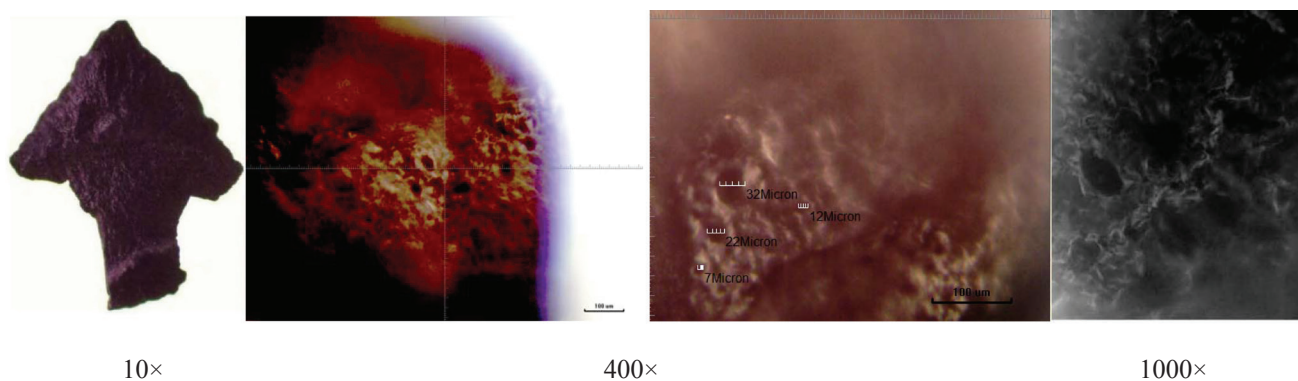


Fig. 2 – Digital microscopic images of ACSTA (10x – 1000x)

### Potentiometric titration

The experimental Boehm titration data of ACS-TA (with 0.1 M NaOH and 0.1 M HCl) is presented as zero-, first-order potentiometric curves and revised as Gran's plots (Fig. 3). Gran's method is based on the transformation of a titration curve into two linear functions vs. the volume of added titrant before and after the end-point titration.<sup>18,19</sup> The intersections of the linear portions with the volume axis correspond to the equivalence points  $V'$  and  $V''$ .<sup>20</sup> Based on these results, the density of the acidic and basic sites on the carbon surface was calculated. The values of the strong, weak, very weak acidic sites, and total basic sites densities are presented in Table 2.

The basic surface sites of activated carbons are usually of Lewis type, associated with  $\pi$  electron-rich regions within the basal planes.<sup>21</sup> Basicity of activated carbons can be associated with: (i) resonating-electrons of carbon aromatic rings that attract protons, and (ii) basic surface functionalities (e.g., N-containing groups) that are capable of binding with protons. It was proposed that certain oxygen containing surface functionalities, such as chromene, ketone, and pyrone, can contribute to the carbon basicity.<sup>22</sup> The predominant acidic sites on biochar surfaces are mainly carboxylic, lactone, and phenolic groups.

### FTIR analyses

The FT-IR spectra of IBU, ACSTA and IBU-loaded ACSTA (Fig. 4) were recorded to outline and analyze the possible interactions between

IBU and the microparticles matrix. The conducted comparative detailed assessment of the characteristic FTIR spectra displayed significant variations in the intensity of relevant bands, clearly indicating the existence of strong interactions between the drug and the excipient.

The FTIR data presented in Table 3 emphasize the influence of the encapsulated biologically active molecules on the spectral characteristics of the carrier. The increased intensities of IBU-ACSTA peaks at 2922 and 1392  $\text{cm}^{-1}$  are attributed to significant  $\text{CH}_2$ - and  $\text{CH}_3$ -symmetric stretching vibrations within IBU molecules. The registered smooth peaks at 2738 and 2679  $\text{cm}^{-1}$ , assigning the presence of O-valence vibrations in the carboxylic OH-group, were solely due to the incorporated drug molecules. Strong  $\text{CH}_3$ -asymmetric deformations and  $\text{CH}_2$ -scissoring of IBU molecules are associated with the band at 1456  $\text{cm}^{-1}$  on the drug-loaded carbon spectrum.

Probable interactions between the organic molecules and ACSTA particles, related to decreased  $\text{CH-CO-}$  and  $\text{OH-in-plane}$  deformations, resulted in reduced intensity of IBU spectral lines at 1420 and 1321  $\text{cm}^{-1}$ , respectively. The latter assumption was supported by the observed increased intensity and area of IBU-ACSTA FTIR bands at 1508, 1541, 1521, 1284, 1147, 1107, 1031, 626 and 420  $\text{cm}^{-1}$  attributed primarily to the aromatic ring C-H, C=C-C in-plane deformations and stretching vibrations of the drug molecules. Possible intermolecular rotations of the ibuprofen molecules during their encapsulation within the solid matrix micropores are the probable reason for the encountered

Table 2 – Acidic and basic surface sites density of ACSTA

Surface sites density	Strong acidic sites, $\text{mmol g}^{-1}$	Weak acidic sites, $\text{mmol g}^{-1}$	Very weak acidic sites, $\text{mmol g}^{-1}$	Total acidic sites, $\text{mmol g}^{-1}$	Total basic sites, $\text{mmol g}^{-1}$	$\text{pH}_{\text{PZC}}$
ACSTA	2.55	0.60	1.87	5.02	6.55	9.6

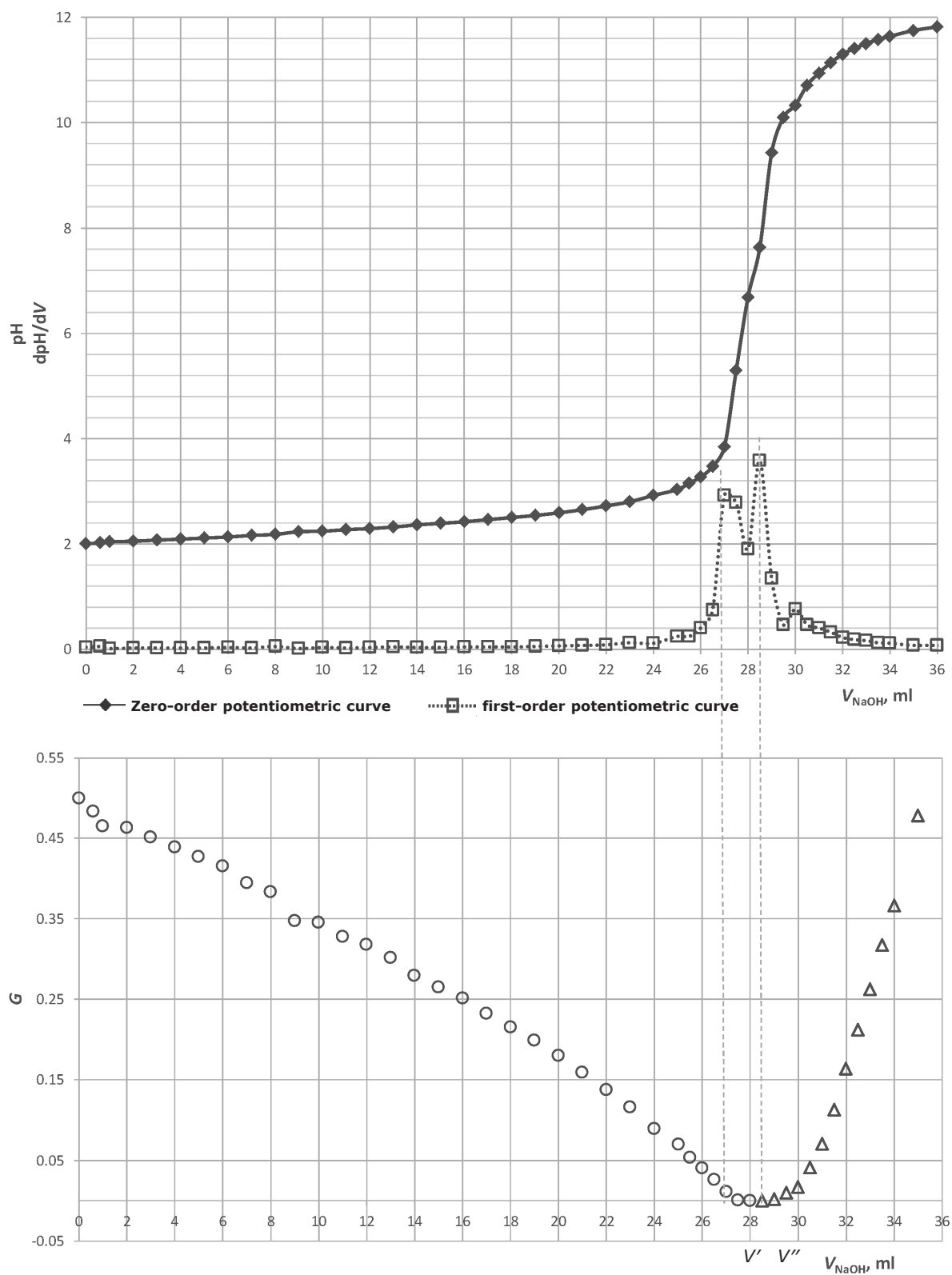


Fig. 3 – Zero-order, first-order potentiometric curves and Grans plot of ACSTA

Table 3 – Characteristic FTIR vibrations and bends of IBU, ACSTA and IBU-loaded ACSTA<sup>23-25</sup>

Bend assignments	Wavenumber, cm <sup>-1</sup>		
	IBU	IBU-loaded ACSTA	ACSTA
OH-stretching	–	3504, 3404, 3276	3444
CH asymmetric stretching	3094, 2958	–	–
CH <sub>2</sub> -symmetric stretching	2868	2922*	2924
CH-stretching vibrations in aliphatic/aromatic groups	–	2852	2850
C≡C-stretching vibrations	–	2351	2362, 2337, 2314
OH O-valence vibrations	2729 2630	2738* 2679*	–
C=O-stretching vibrations	1722	1716*	–
C=O-stretching vibrations in aldehyde/keto/ carboxylic groups and quinones	–	1697–1616	1700–1630
aromatic C=C stretching	1507	1508* 1541, 1521	1552, 1514
CH <sub>3</sub> -asymmetric deformations; CH <sub>2</sub> -scissoring	1462	1456*	1452
CH–CO-deformations	1420	1417*	1421
CH <sub>3</sub> -symmetric stretching	1380	1392*	–
C=O/C–O-stretching in carboxylic groups	–	1373–1361	1377–1363
OH-in-plane deformations	1321	1328*	1332
=C–H-in-plane deformations	1268	1284*	–
C–C-stretching vibrations	1230	1245*	–
C–O-stretching vibrations	1183	1184*	–
=C–H-in-plane deformations	1122, 1067	1147*, 1107*, 1031*	–
C–O-stretching vibrations	970	972*	974
C–H-out-of-plane vibrations	866	864*	merged peaks
CH <sub>2</sub> -rocking vibrations	779	771*	765
C–H-out-of-plane deformations	668	673*	670–676 merged peaks
C–H-in-plane ring deformations	636	626*	640
C–C deformations; CH <sub>2</sub> -in-plane rocking; CH <sub>2</sub> -/CH <sub>3</sub> -deformation vibrations	600–460	600–450	600–450
C=C–C-aromatic ring asymmetric bending; C–H-out-of-plane aromatic ring bending	421	420* 452	420 457

\*FTIR vibrations attributed to IBU

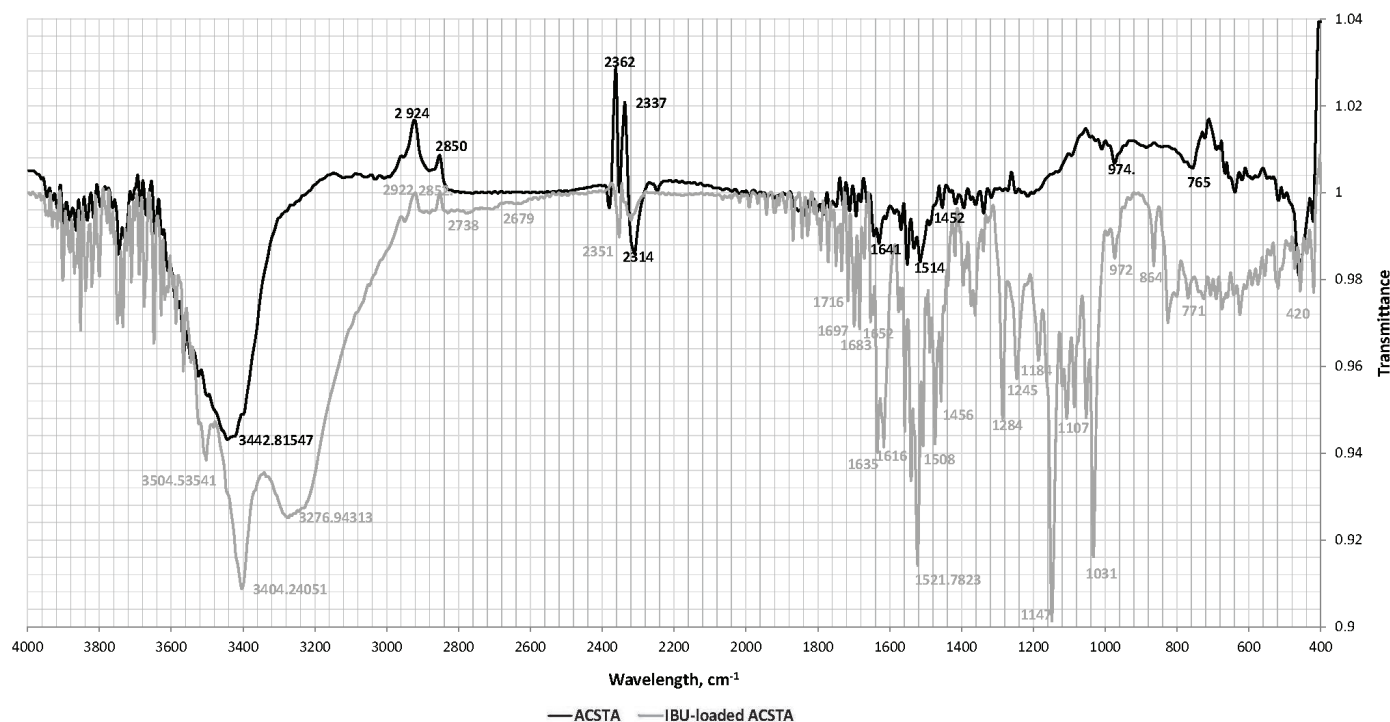


Fig. 4 – FTIR spectra of fresh and IBU-loaded ACSTA

C–H–out-of-plane vibrations and deformations at 864 and 673  $\text{cm}^{-1}$  on the IBU-loaded carbon spectrum. The comparative analyses of the FT-IR spectra of IBU, ACSTA and IBU-loaded ACSTA revealed that, in the prepared NSAID/carbon carrier system, the strong bands assigned to the vibration of the drug molecules were predominant, which provided evidence for the high extent of IBU encapsulation in the carbon matrix.

### Equilibrium study

To assess the versatility and tuneability of drug loading, investigations on the encapsulation behavior of the biologically active molecules on the studied solid microcarrier at equilibrium conditions are essential. In the present study, the highest achieved ACSTA encapsulation efficiency towards IBU at equilibrium conditions was  $E = 52\%$ , and the maximum equilibrium capacity –  $q_e^{\text{max}} = 19.5 \mu\text{g IBU mg}^{-1}$  ACSTA (Fig. 5a).

The experimental equilibrium data were described by five mathematical models by non-linear regression analyses. The values of the calculated isotherm parameters and error functions are presented in Table 4. The comparative analyses of the mode of the experimental and model isotherms (Fig. 5b) supported by the highest  $R^2$  and the lowest SSE and chi-square ( $\chi^2$ ) values determined that the four-parameter Baudu model presented the best description of the encapsulation behavior of the NSAID on the activated carbon. The adsorption isotherm had concave shape in the region of small

equilibrium concentrations of IBU as a result of weak affinity of non-polar aromatic ring to polar OH-groups, but then followed a sharp increase of aromatic uptake. Obviously, it could be explained by the reorientation of the drug molecules owing to their increased concentration in the solution, thus it was easier for additional amounts to become fixed as a result of hydrophobic interaction.<sup>26</sup> Baudu isotherm model has been developed mainly due to the rise of discrepancy in calculating Langmuir constant and coefficient over a broad range of concentrations. Baudu isotherm model is the transformed form of the Langmuir isotherm. This model is only applicable in the range of  $(1+x+y) < 1$  and  $(1+x) < 1$ . For lower surface coverage, Baudu model reduces to the Freundlich equation.

The monolayer sorption capacity ( $q_B = 1.435 \text{ mg g}^{-1}$ ) predicted by Baudu model, was lower than the experimentally obtained. However, according to the plots in Fig. 5b, this model isotherm seemed to be the best-fitting model with regard to the experimental equilibrium data. It displays the best representation of the equilibrium behavior of the system in the low concentration range. At higher concentrations, Baudu isotherm nearly coincides with the multilayer isotherm. However, due to the increased number of isotherm parameters in the four-parameter Baudu model, it simulates the model variations more accurately. In the case of sorptive processes of organic macromolecules like drugs having different types of functional groups, the factors affecting sorption are large. Therefore, in the absence of a theoretical model that could account for the chemi-

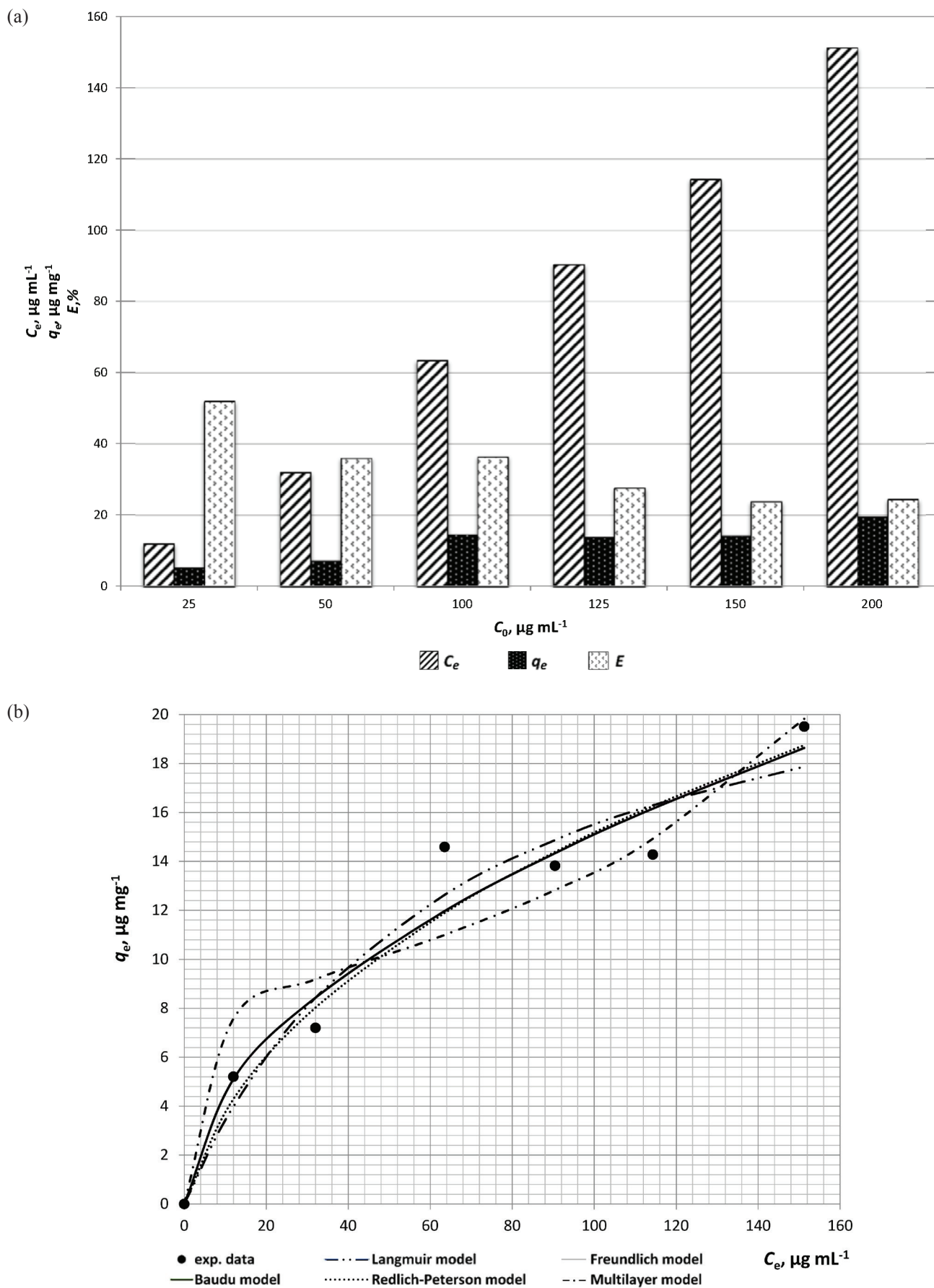


Fig. 5 – a) Equilibrium drug concentration, encapsulation capacity, and efficiency for the system IBU/ACSTA; b) Experimental and model isotherms of the system IBU/ACSTA

Table 4 – Values of the equilibrium model parameters and error functions<sup>16,27,28</sup>

Equilibrium model	Isotherm parameters	Error functions
Langmuir $q_e = \frac{K_L c_e}{1 + a_L c_e} \quad (3)$ Linear form: $\frac{c_e}{q_e} = \frac{1}{K_L} + \frac{a_L}{K_L} c_e \quad (4)$	$q_m = 25.551$ $K_L = 0.383$ $a_L = 0.015$	$R^2$ 0.945 SSE 14.651 MSE 2.930 RMSE 1.712 $\chi^2$ 1.2582
Freundlich $q_e = K_F \cdot c_e^{n_F} \quad (5)$	$K_F = 1.435$ $n_F = 0.511$	$R^2$ 0.908 SSE 12.922 MSE 3.230 RMSE 1.797 $\chi^2$ 0.9863
Redlich-Peterson $q_e = \frac{K_R c_e}{1 + a_R c_e^b} \quad (6)$	$K_R = 0.786$ $a_R = 0.276$ $b = 0.59$	$R^2$ 0.951 SSE 13.582 MSE 3.396 RMSE 1.843 $\chi^2$ 1.0774
Multilayer $q_e = \frac{Q_m K_1 c_e}{(1 - K_2 c_e)[1 + (K_1 - K_2) c_e]} \quad (7)$ Second-order polynomial form: $\frac{c_e}{q_e} = \frac{c_e^2 (K_2^2 - K_1 K_2) + c_e (K_1 - 2K_2) + 1}{Q_m K_1} \quad (8)$	$Q_m = 8.611$ $K_1 = 0.417$ $K_2 = 0.414$	$R^2$ 0.913 SSE 23.930 MSE 5.983 RMSE 2.446 $\chi^2$ 2.7166
Baudu $q_e = \frac{q_B b_B c_e^{(1+x+y)}}{1 + b_B c_e^{(1+x)}} \quad (9)$	$q_B = 1.435$ $b_B = 223.786$ $x = 75.957$ $y = 0.511$	$R^2$ 0.953 SSE 12.922 MSE 4.307 RMSE 2.075 $\chi^2$ 0.9863

cal heterogeneity of the surface, and simultaneous prevalence of different sorption mechanisms, isotherm models having a greater number of model constants are able to predict the system behavior better.

### Kinetics of IBU encapsulation

Drug release and its relationship with the kinetics parameters of drug sorption onto ACSTA micro-particles have been studied using IBU as a model drug. The sorption method is more flexible and can avoid limitations or problems which occur with molten or dissolution methods. To understand drug release sorption loading, kinetics and apparent mass transfer parameters, such as mass-transfer and diffusion coefficients have been investigated. In this

respect, six diffusion and kinetics models were applied to describe the experimental data. Their applicability was ranked on the bases of the calculated regression coefficients and error functions by the linear/non-linear approach. According to the experimental kinetics curve, equilibrium between the incorporated and released drug molecules was reached after 200 min.

The values of the calculated model parameters and error functions are presented in Table 5. According to the analyses of these data and the comparison of the modes of the experimental and model kinetics curves, it was established that the pseudo-first order, the mixed pseudo first-second order, and the intraparticle diffusion models characterized with the lowest applicability.

Table 5 – Values of the kinetics/diffusion models parameters and error functions<sup>30–34</sup>

Kinetics model	Kinetics parameters	Error functions
Pseudo-first order model Non-linear form $\frac{dq_t}{dt} = k_1 \cdot (q_e - q_t)$ (10) Linear expression $\log(q_e - q_t) = \log q_e - \frac{k_1}{2.303} \cdot t$ (11)	$k_1 = 0.0211$ $q_{e1} = 15.559$	$R^2$ 0.888 MSE 0.075 RMSE 0.273
Pseudo-second order model Non-linear form $\frac{dq_t}{dt} = k_2 \cdot (q_e - q_t)^2$ (12) Linear expression $\frac{1}{q_t} = \frac{1}{k_2 \cdot q_e^2} + \frac{1}{q_e} \cdot t$ (13)	$k_2 = 0.0027$ $q_{e2} = 19.885$ $h = 1.068 \mu\text{g mg}^{-1} \text{min}^{-1}$	$R^2$ 0.968 MSE 0.626 RMSE 0.791
Mixed pseudo first-second order model Non-linear form $q_t = q_e \left( \frac{1 - \exp(-k_1 \cdot t)}{1 - f_2 \cdot \exp(-k_1 \cdot t)} \right)$ (14) Linear expression $\ln \left( \frac{1 - F}{1 - f_2 \cdot F} \right) = -k_1 \cdot t$ (15) where $F = \frac{q_t}{q_e}$ (16) $f_2 = \frac{k_2 \cdot q_e}{k_1 + k_2 \cdot q_e}$ (17)	$k_{\text{MO1}} = -0.013$ $k_2 = 5.245 \cdot 10^{-3}$ $f_2 = 1.143$	$R^2$ 0.952 MSE 0.005 RMSE 0.072
Elovich model Non-linear form $\frac{dq}{dt} = \alpha \cdot \exp(-\beta \cdot q_t)$ (18) Linear expression $q_t = \frac{1}{\beta} \cdot \ln(\alpha \cdot \beta) + \frac{1}{\beta} \cdot \ln(t)$ (19)	$\alpha = 6.720 \mu\text{g mg}^{-1} \text{min}^{-1}$ $\beta = 0.321 \text{mg } \mu\text{g}^{-1}$	$R^2$ 0.961 MSE 1.427 RMSE 1.195
Intraparticle diffusion model Non-linear form $q_t = k_i \cdot t^{0.5} + I$ (20)	$k_{i1} = 1.734$ $I_1 = 3.226$ $k_{i2} = 0.145$ $I_2 = 13.385$ $k_{i3} = 1.135$ $I_3 = 3.208$	$R_{i1}^2$ 0.865 MSE 2.749 RMSE 1.658 $R_{i2}^2$ 0.960 MSE 0.013 RMSE 0.115 $R_{i3}^2$ 0.783 MSE 3.681 RMSE 1.919
Mixed surface reaction and diffusion controlled kinetics model	$k = 6.803 \cdot 10^{-5} \text{mL } \mu\text{g}^{-1} \text{min}^{-1}$ $\tau = 58 \text{min}$ $u_{eq} = 0.706$	$R^2$ 0.968 MSE 1.651 RMSE 1.285

where:  $k_1$  – rate constant of first order kinetics;  $q_{e1}$  – sorption capacity of first order kinetics,  $\mu\text{g mg}^{-1}$ ;  $k_2$  – rate constant of second order kinetics;  $q_{e2}$  – sorption capacity of second order kinetics,  $\mu\text{g mg}^{-1}$ ;  $k_i$  – rate constant for intraparticle diffusion;  $I$  – model constant in the intraparticle diffusion model;  $\alpha$  – initial sorption rate in Elovich model;  $\beta$  – desorption constant in Elovich model;  $k$  – rate coefficient  $\text{mL } \mu\text{g}^{-1} \text{min}^{-1}$ ;  $\tau$  – coefficient related to diffusion;  $u_{eq}$  – relative equilibrium uptake;  $\alpha$  – initial sorption rate,  $\mu\text{g mg}^{-1} \text{min}^{-1}$ ;  $\beta$  – desorption constant related to surface coverage and activation energy for chemisorption,  $\text{mg } \mu\text{g}^{-1}$ .

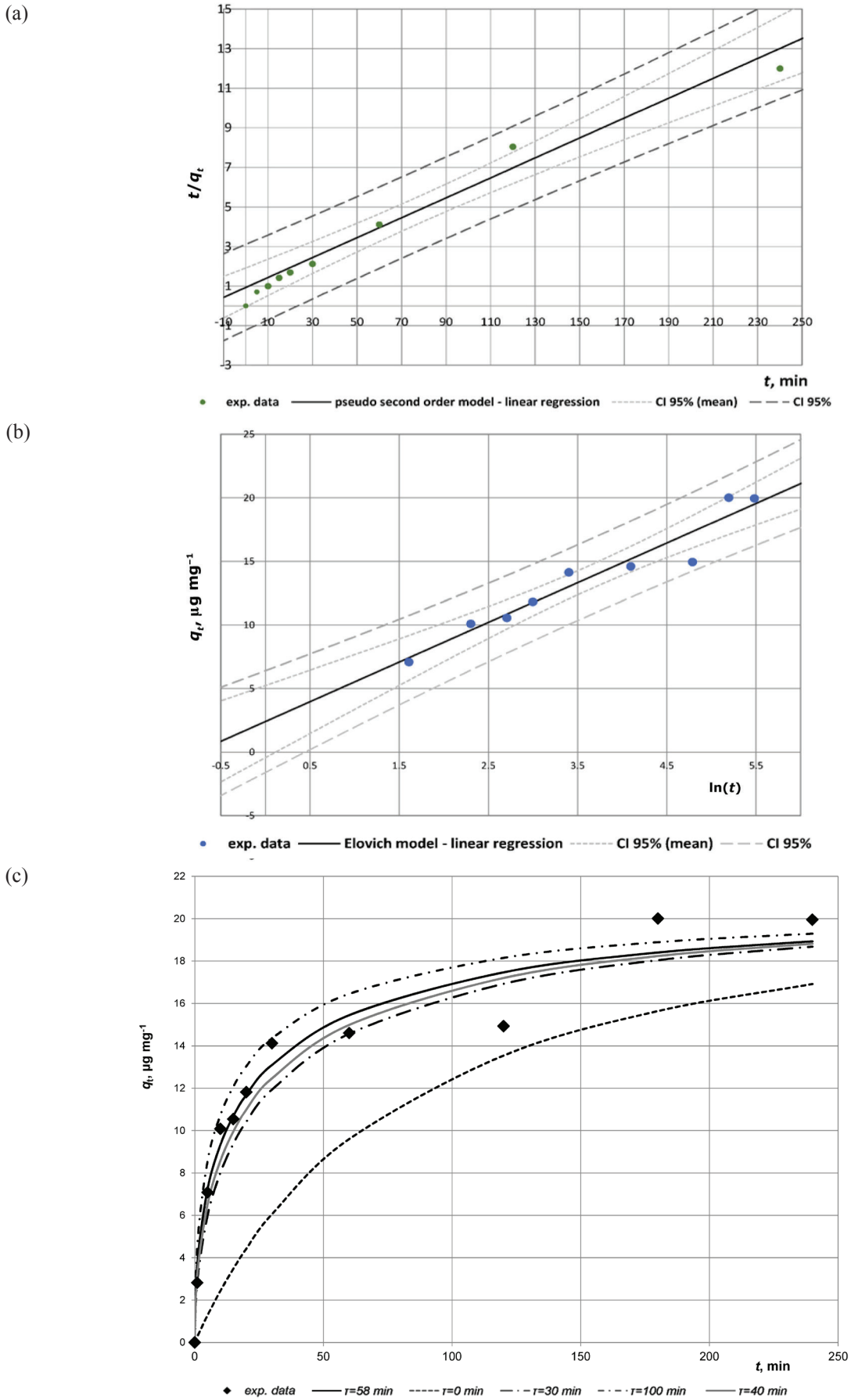


Fig. 6 – Linear form of a) pseudo-second order, b) Elovich kinetics models, and c) mixed surface reaction and diffusion controlled kinetics model

The experimentally demonstrated observation of the sorption rate slowing down with time is explained by the Elovich model according to which, at first, the lower energy surface sites of the carbon saturate, and then the adsorption, shifts to the higher energy surface sites, resulting in a decrease in the sorption rate. The Elovich equation is known to describe chemisorption well, similarly to the assumptions of the pseudo-second order model, although the initial sorption rate predicted by the Elovich equation ( $\alpha = 6.720 \mu\text{g mg}^{-1} \text{min}^{-1}$ ) is approximately 6 times greater than that determined by the pseudo-second order one ( $h = 1.068 \mu\text{g mg}^{-1} \text{min}^{-1}$ ). Besides, the Elovich model accounts for the role of desorption expressed by the desorption constant ( $\beta = 0.321 \text{mg } \mu\text{g}^{-1}$ ) related to surface coverage and activation energy for chemisorption (Table 5). Both kinetics models characterized with significantly high values of the correlation coefficient (Fig. 6a, b; Table 5). The Elovich model is physically unsound as it predicts infinite sorption capacity at long periods of time. Therefore, it is suitable for kinetics far from equilibrium where desorption does not occur because of low surface coverage.<sup>29</sup> The mixed surface reaction and diffusion controlled kinetics model considers both diffusion and surface reaction as the rate-controlling steps. The significant effect of diffusion on the overall sorption process is determined by the value of the parameter  $\tau$  (Table 5). To derive the equation that best fits the experimental data, an iteration procedure with  $0 \leq \tau \leq 100$  was conducted. The model curves presented in Fig. 6c, the values of the calculated model parameters and error functions (Table 5) proved that the experimental kinetics behavior of the studied drug/carrier system was best described at  $\tau = 58$  min. Consequently, it could be considered that IBU molecules diffuse toward ACSTA active sites and then, after 58 min contact time, they adsorb on the surface sites through a surface reaction mechanism.

### Mass transfer mechanism of IBU encapsulation

The effect of the mass transfer mechanisms through the boundary layer fluid-solid phase and the diffusion of IBU molecules during the drug encapsulation on ACSTA microparticles were assessed by determination of the values of the characteristic mass transfer and diffusion parameters. The external mass transfer coefficient,  $k_p$ , calculated by McKay and Weber-Mathews equations, characterized with significantly higher value as compared to the partial solid-phase mass transfer coefficient,  $k_s$  (Table 6). The latter indicates that the resistance which the solid phase renders to the drug molecules, significantly overlaps the boundary layer resistance. The mass transfer resistances were also analyzed by estimating the Biot number – Eq. (21), which is a

dimensionless criterion for the predominance of external surface mass transfer against solid phase intraparticle diffusion.

$$Bi = \frac{k_f \cdot r_p}{D_{eff}} \quad (21)$$

The determination of the effective diffusivity coefficient,  $D_e$ , in Eq. (28) (Table 6) requires the calculation of the values of the solid phase diffusion,  $D_s$ , and pore diffusion,  $D_p$ , coefficients (Table 6). The value estimated in the present study of  $D_e = 5.744 \cdot 10^{-12} \text{m}^2 \text{s}^{-1}$  for IBU is approximately 10 times greater than the values of this coefficient for acetaminophen, diclofenac and sulfamethoxazole  $D_e = 2.63\text{--}9.33 \cdot 10^{-13} \text{m}^2 \text{s}^{-1}$ .<sup>34</sup>

It is accepted that, for  $Bi$  numbers  $< 0.5$ , the sorption process is limited by external mass transfer. As the value of  $Bi$  obtained in the present study was above 100, it could be concluded that the process of IBU encapsulation on ACSTA microparticles was controlled predominantly by intraparticle solid phase diffusion.

### *In vitro* release study

The use of *in vitro* drug dissolution data to predict *in vivo* bioavailability of pharmaceutical formulations can be considered as the rational development of controlled release systems. Model-dependent methods are based on various assumptions and imply mathematical functions, which describe the dissolution profile. Once a suitable function had been selected, the dissolution profiles were evaluated depending on the derived model parameters.

Pepsin-free simulated gastric fluid was used for the *in vitro* release study, as the main aim of the research was to assess the encapsulation and release efficiency of ACSTA towards IBU. In this respect, the addition of an enzyme would cause degradation of the drug and lead to the release of its metabolic products, which would affect the required results.

According to the experimental data, the highest extent of IBU release from ACSTA microparticles in simulated gastric fluid solution was  $134.31 \mu\text{g mL}^{-1}$ , which was equal to desorption efficiency  $E_{des}$  54.1 % at 298 K achieved after 1200 min. The experimentally determined IBU concentration in the ACSTA matrix before its release was  $117.1 \text{mg g}^{-1}$ .

To outline the suitable release kinetics model describing the dissolution profile of IBU, nonlinear regression was applied. The experimental results from the *in vitro* desorption studies in simulated gastric fluid (pH = 1.2) were modelled by the Higuchi, Korsmeyer-Peppas, Weibull, and Peppas-Sahlin models. The values of the model parameters and error functions are presented in Table 7.

Table 6 – Values of the mass transfer and diffusion coefficients of IBU encapsulation

Parameter	Value	Equation
Particle porosity, $\varepsilon_p$ , –	0.34	
Particle density, $\rho_p$ , g cm <sup>-3</sup>	576	
Particle surface area, $S_p$ , m <sup>2</sup>	2.1·10 <sup>-7</sup>	
Microcarrier concentration, $m_s$ , g dm <sup>-3</sup>	6.67	
External mass transfer coefficient, $k_f$ , m s <sup>-1</sup>		McKay equation
	1.44·10 <sup>-4</sup>	$\frac{C_t}{C_0} = \frac{1}{1 + m_s K_L} + \frac{m_s \cdot K_L}{1 + m_s \cdot K_L} \exp\left(-\frac{1 + m_s K_L}{m_s \cdot K_L} k_f S_p t\right)$ (22)
		Weber-Mathews equation:
	4.90·10 <sup>-4</sup>	$\frac{d\left(\frac{C}{C_0}\right)}{dt} = -k_f \cdot S_p$ (23)
Intraparticle mass transfer		
Solid phase diffusion coefficient, $D_s$ , m <sup>2</sup> s <sup>-1</sup>		Weber-Morris equation:
	3.169·10 <sup>-13</sup>	$\frac{q_t}{q_e} = 6 \left(\frac{D_s \cdot t}{r_p^2}\right)^{\frac{1}{2}} \left(\pi^{-\frac{1}{2}} + L\right)$ (24)
		Crank equation:
	1.902·10 <sup>-12</sup>	$\frac{q_t}{q_e} = 1 - \frac{6}{\pi^2} \exp\left(-\frac{D_s \cdot t \cdot \pi^2}{r_p^2}\right)$ (25)
Pore diffusion coefficient, $D_p$ , m <sup>2</sup> s <sup>-1</sup>		Mackie-Meares equation:
	5.744·10 <sup>-12</sup>	$D_p = \left(\frac{\varepsilon_p}{2 - \varepsilon_p}\right)^2 \frac{D_m}{\varepsilon_p}$ (26)
Molecular diffusion coefficient, $D_m$ , m <sup>2</sup> s <sup>-1</sup>		Wilke-Chang equation:
	7.36·10 <sup>-12</sup>	$D_m = \frac{1 \cdot 10^{-6}}{A \cdot B \cdot \sqrt{\mu_w \left(\frac{1}{\rho_A^3} + \frac{1}{\rho_B^3}\right)^2}} \sqrt{\frac{1}{M_A} + \frac{1}{M_B}}$ (27)
Ibuprofen molecular volume, $v_A$ , Å <sup>3</sup>	198.96	
Ethanol molecular volume, $v_B$ , Å <sup>3</sup>	48.45	
Wilke-Chang coefficient for EtOH, $B$	2.00	
Effective diffusivity coefficient, $D_e$ , m <sup>2</sup> s <sup>-1</sup>	5.744·10 <sup>-12</sup>	Crank equation:
		$D_{eff} = D_p + K_{ads} D_s$ (28)
		$D_p = \frac{D_m}{\tau_p}$ (29)
Adsorption coefficient, $K_{ads}$ , m <sup>3</sup> g <sup>-1</sup>	0.254·10 <sup>-3</sup>	$K_{ads} = \frac{\rho_p}{\varepsilon_p} K$ (30)
Partial solid-phase mass transfer coefficient, $k_s$ , m s <sup>-1</sup>	3.804·10 <sup>-8</sup>	$k_s S_p = \frac{15 D_s}{r_p^2}$ (31)

where  $\rho_p$  is particle density, g cm<sup>-3</sup>;  $\varepsilon_p$  – particle porosity, –;  $K$  – linear isotherm slope, dm<sup>3</sup> g<sup>-1</sup>;  $\tau_p$  – pore tortuosity factor ( $\tau_p = 2 - 6$ );  $D_m$  – Wilke-Chang equation;  $\mu_w$  – viscosity of water, Pa s;  $v_A$  – molecular volume of the drug in Wilke-Chang equation, cm<sup>3</sup> g<sup>-1</sup> mol<sup>-1</sup>;  $v_B$  – molecular volume of EtOH in Wilke-Chang equation, cm<sup>3</sup> g<sup>-1</sup> mol<sup>-1</sup>;  $M_A$  – molecular weight of IBU, g mol<sup>-1</sup>;  $M_B$  – molecular weight of EtOH, g mol<sup>-1</sup>;  $A$  – coefficient characterizing the solute ( $A = 1.0$  for non-associated liquids);  $B$  – coefficient characterizing the solvent ( $B = 4.3$  for water).

Table 7 – Release models parameters and error functions

Model	Parameters	Error functions			
Zero-order model $C_t = C_0 + k_0 \cdot t$ (32)	$k_0 = 0.144$	$R^2$	0.676		
		SSE	11502		
		MSE	1643.2		
		RMSE	40.534		
Higuchi model $C_t = [2 \cdot D \cdot S \cdot \varepsilon (A - 0.5 \cdot S \cdot \varepsilon)]^{0.5} \cdot t^{0.5}$ (33)	$K_H = 4.549$	$R^2$	0.866		
		SSE	2871.73		
		MSE	410.25		
		RMSE	20.255		
Simplified form: $C_t = K_H \cdot t^{1/2}$ (34)					
Korsmeyer-Peppas model $\frac{C_t}{C_\infty} = k_{KP} \cdot t^n$ (35)	at $C_t/C_0 < 0.6$ $k_{KP} = 0.002$ $n = 1.235$	at $C_t/C_0 > 0.6$ $k_{KP} = 0.224$ $n = 0.211$	at $C_t/C_0 < 0.6$ $R^2$ 0.999 SSE $1.39 \cdot 10^{-4}$ MSE $1.39 \cdot 10^{-4}$ RMSE 0.012	at $C_t/C_0 > 0.6$ $R^2$ 0.999 SSE $5.98 \cdot 10^{-5}$ MSE $2.99 \cdot 10^{-5}$ RMSE 0.005	
Weibull model $C_t = C_0 \cdot \left[ 1 - e^{-\frac{(t-T)^b}{a}} \right]$ (36)	at $b = 1.0$ $C_0^{mod} = 124.10$ $a = 125$ $t = 7.802$	at $b = 0.2$ $C_0^{mod} = 56.68$ $a = 3.289$ $t = 15$	at $b = 1.0$ $R^2$ 0.967 SSE 0.038 MSE 0.008 RMSE 0.087	at $b = 0.2$ $R^2$ 0.901 SSE 0.119 MSE 0.024 RMSE 0.154	
Peppas-Sahlin model $\frac{C_t}{C_0} = k_{1PS} \cdot t^m + k_{2PS} \cdot t^{2 \cdot m}$ (30)	$k_{1PS} = 0.0769$ $k_{2PS} = 2.709 \cdot 10^{-5}$ $m = 0.371$		$R^2$	0.895	
			SSE	0.134	
			MSE	0.022	
			RMSE	0.149	

$C_t$  – cumulative amount of drug released in time  $t$ ;  $C_0$  – initial amount of drug in solution (usually  $C_0 = 0$ );  $k_0$  – zero-order release constant;  $D$  – diffusion coefficient of the drug molecule in the solvent in Higuchi model;  $\varepsilon$  – porosity of the matrix;  $S$  – surface area;  $K_H$  – release rate constant in the Higuchi model;  $k_{KP}$  – release constant incorporating structural and geometric dosage from characteristics in Korsmeyer-Peppas model;  $n$  – the release exponent indicating the drug release mechanism in Korsmeyer-Peppas model;  $a$  – time process parameter in Weibull model;  $t$  – lag time (in most cases zero);  $b$  – shape parameter in Weibull model: characterizes the curve as exponential ( $b=1$ ), S-shaped with upward curve followed by turning point ( $b>1$ ), or parabolic with higher initial slope, after that consistent with the exponential ( $b<1$ );  $k_{1PS}$  and  $k_{2PS}$  – kinetics coefficients in Peppas-Sahlin model;  $m$  – diffusional exponent in Peppas-Sahlin model.

The Higuchi model gave no significant correlation towards the experimental data, which was consistent with the low  $R^2$  and high SSE, MSE and RMSE values determined by non-linear regression analyses (Table 7).

According to Table 7, the Peppas-Sahlin model characterized with better applicability as compared to the Higuchi model. The first term of the model considers the contribution of Fickian diffusion, while the second – case II relaxation. The exponential coefficient  $m$  relates to the purely Fickian diffusion exponent. The ratio of relaxational ( $R$ ) over Fickian contribution ( $F$ ) can be calculated by the following expression:<sup>36</sup>

$$\frac{R}{F} = \frac{k_{1PS}}{k_{2PS}} \cdot t^m \quad (38)$$

The plot of  $R/F$  vs.  $t$  is presented in Fig. 7. According to the model assumptions, when  $R/F = 1$ , the release mechanism contains both erosion and diffusion equally; at  $R/F > 1$  the relaxation (ero-

sion) dominates, while for  $R/F < 1$ , the rate-limiting role of Fickian diffusion dominates.

The Weibull model characterized with relatively high value of the regression coefficient and acceptably low values of the other three error functions, which proved its applicability towards the experimental data. The Weibull function predicts a general trend for free diffusion at short times tending toward fractal space, i.e., geometry controlled, diffusion with increasing time. The shape parameter,  $b$ , characterizes the curve as either exponential ( $b = 1$ ), S-shaped with upward curvature followed by a turning point ( $b > 1$ ), or as one with a steeper initial slope than was consistent with the exponential ( $b < 1$ ). The experimental data of IBU release from ACSTA microparticles were best fitted by the model at  $b = 1$  (Fig. 8a). The time parameter,  $t$  represents the time interval necessary for 63.2 % drug release. According to the modes of the experimental and Weibull release kinetics curves in Fig. 8a, obviously the model characterizes with higher extent of applicability in the initial stages of the release process.

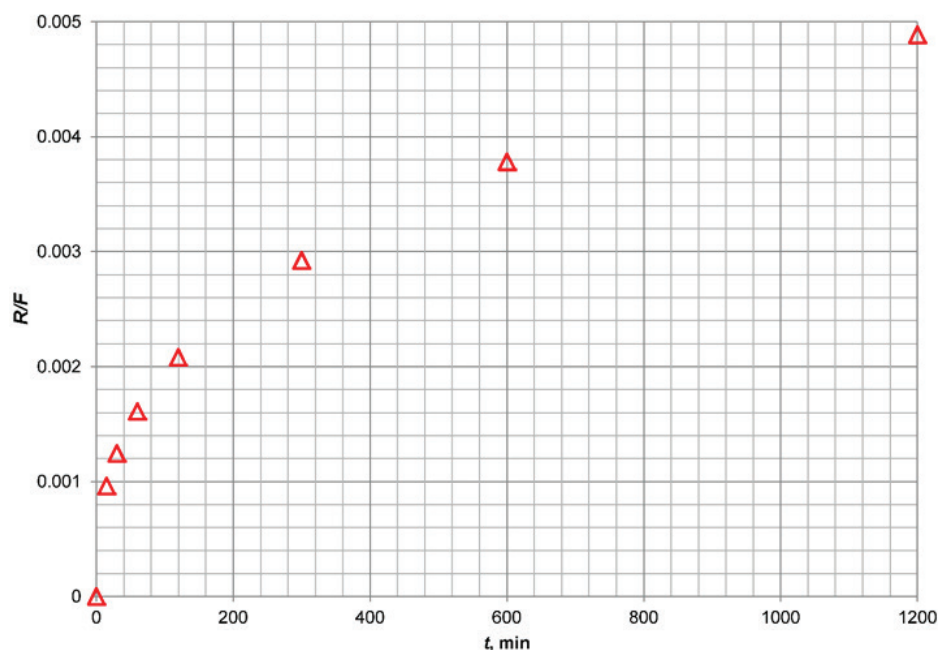


Fig. 7 – Relaxation contribution ( $R$ )/Fickian diffusion contribution ( $F$ ) ratio with respect to time

According to the values of the correlation coefficients and error functions, the Korsmeyer-Peppas model displayed the best applicability towards the experimental release results (Table 7, Fig. 8b). The semi-empirical model of Korsmeyer-Peppas is applied for analyses of the release of pharmaceutical cylindrical shaped dosage forms, when the release mechanism is not well known or when more than one type of release could be involved. The value of the parameter  $n$  in the equation is indicative of the diffusion mechanism: for  $0.45/0.5 \leq n$  corresponds to a Fickian diffusion mechanism,  $0.45/0.5 < n < 0.89$  to non-Fickian transport,  $n = 0.89$  to relaxational transport, and  $n > 0.89$  to super case II transport. The applicability of the model to the experimental data at different values of  $n$  was evaluated in the entire concentration range  $0 < C_t/C_0 < 1$  (Fig. 8b). The analyses of the results outlined that the experimental data could not be significantly correlated with a single  $n$  value for the entire concentration interval, which in turn is indicative of the presence of more than one release mechanism. A boundary value of  $C_t/C_0 \sim 0.6$  distinguishing the probable rate-controlling mechanisms in the initial and later stages of the release process was defined. The value of  $n$  determined at  $C_t/C_0 < 0.6$  in the current study was  $n = 1.235$ , which demonstrated the complex influence of probable abrasion of the solid microcarrier due to mechanical scraping of the surface by friction between the moving particles and diffusion on the release of the organic substance during the initial stages of the process. At  $C_t/C_0 > 0.6$ , the value of  $n$  was 0.211, which proved undoubtedly the limiting role of Fickian diffusion mechanism during the later stages of the process.

### Host-guest interactions

The presence of inter- and intramolecular non-covalent interactions and bonded structures between drugs and carrier-matrices are identified as a key factor affecting drug encapsulation and release.<sup>37</sup> In addition, numerous factors, such as drug-carrier interaction, morphology of the matrix, porosity, and carrier concentration can influence the complex processes of the encapsulation and release profile of drugs.

Ibuprofen characterizes as a weak acid ( $pK_a = 4.91$ ) with poor solubility in water and very good solubility in ethanol and methanol. Its physicochemical and molecular characteristics are presented in Table 8. The molecule contains an asymmetric C-atom in the propionic acid residue, which determines the presence of two enantiomers: the S-enantiomer having analgesic and anti-inflammatory activity, and the R-isomer, which is inert. As a result of molecular modeling, IBU molecule was characterized by the following dimensions: 1.03 nm (length), 0.52 nm (width), 0.43 nm (thickness).<sup>38</sup>

Table 8 – Physicochemical and molecular properties of IBU

Chemical formula	$C_{13}H_{18}O_2$
Molecular mass	206.29 g mol <sup>-1</sup>
Density	1.03 g cm <sup>-3</sup>
Melting temperature	75 to 78 °C
Boiling temperature	157 °C
Solubility in water	0.021 mg mL <sup>-1</sup> (20 °C)
Dissociation constant	$K_a = 1.2 \cdot 10^{-5}$ (25 °C)

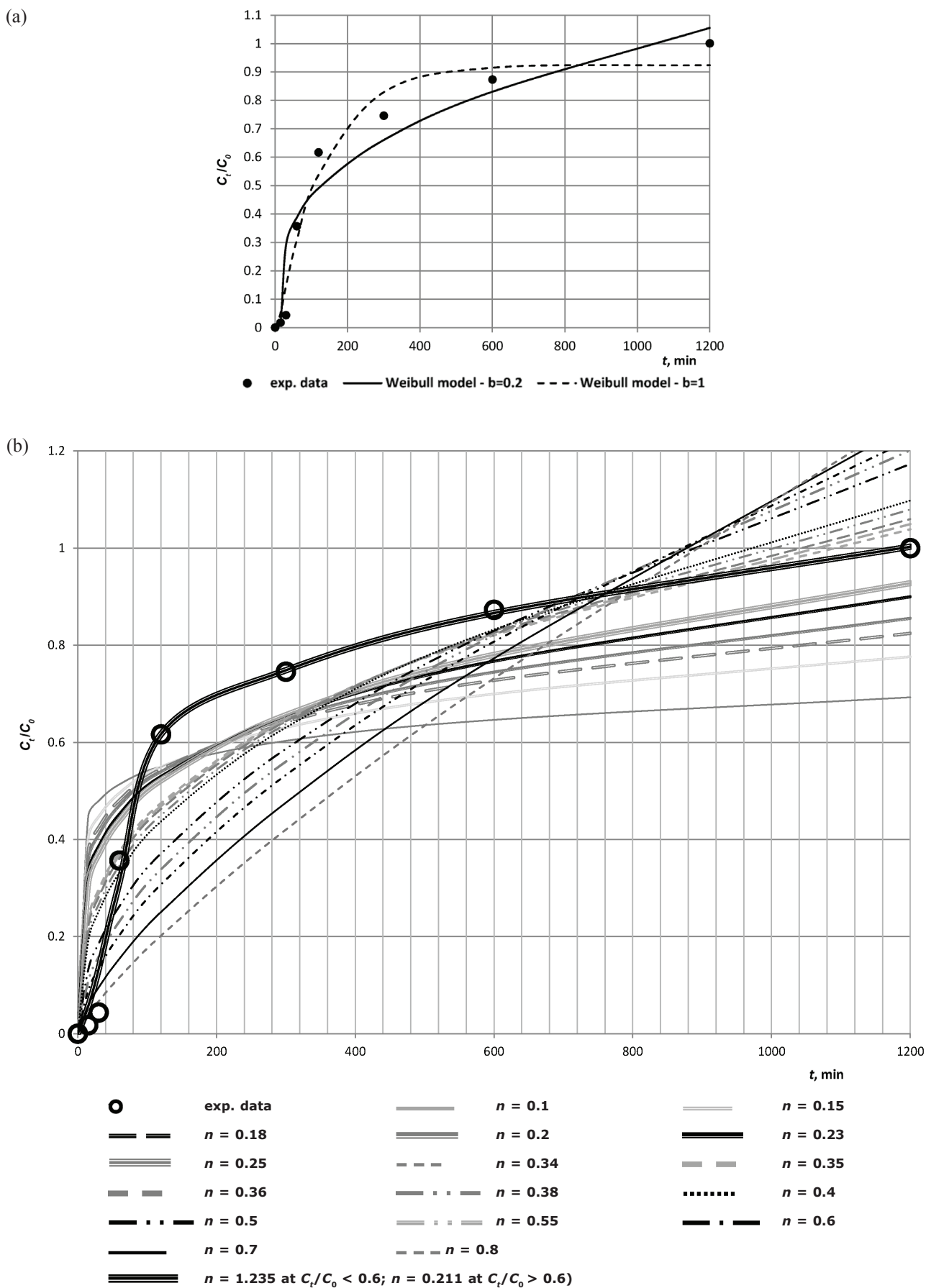
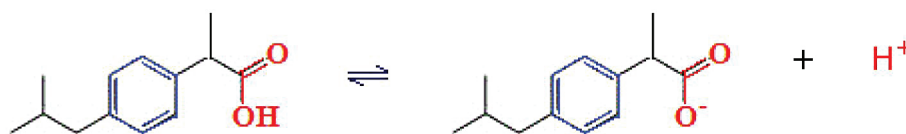


Fig. 8 – Fit of drug dissolution data with: a) Weibull release model, and b) Korsmeyer-Peppas release model

IBU dissociation in aqueous solution proceeds as follows:



The organic molecule contains a polar carboxylic group ( $-\text{COOH}$ ), but the available non-polar alkyl groups and the benzene ring significantly reduce the polarity of the organic molecule. The comparative analysis of the physicochemical, spectral characteristics of the organic molecule, the surface properties of the microcarrier, as well as the kinetic encapsulation and release of the biologically active substance led to the conclusion that the interaction between IBU molecules and ACSTA microparticles was due to electrostatic and dispersion intermolecular forces, as well as formation of H-bonds. Although the hydrogen bond is a weak interaction, Hao and Li found that a substantially high number of hydrogen bond formations could decrease drug release rate.<sup>39,40</sup> The major active moieties of ACSTA microparticles are  $-\text{OH}$  and  $-\text{COOH}$  surface groups that interact with polar molecules and various functional groups in the structure of the organic molecules. The surface electrically charged groups of the carrier are:  $-\text{OH}_2^+$  at  $\text{pH} < \text{pH}_{\text{PZC}}$ ;  $-\text{O}^-$  at  $\text{pH} > \text{pH}_{\text{PZC}}$ , and electroneutral  $-\text{OH}$  at  $\text{pH} \approx \text{pH}_{\text{PZC}}$ . In alkaline medium repulsion forces between the surface  $\text{OH}^-$  of ACSTA and the anionic  $-\text{COO}^-$  groups of O would act, but since IBU molecules are predominantly non-dissociated in EtOH solution, the effect of these interactions in the system under examination is insignificant. According to Pawlish *et al.*, the use of  $\pi$ - $\pi$  stacking, although with relatively low strength, can still improve the encapsulation proper-

ties and stability of the carriers towards loading of drugs containing aromatics.<sup>37</sup> In the present study, the high degree of encapsulation of IBU on AB microparticles is indicative of dominant hydrophobic interactions:  $\pi$ - $\pi$  interactions due to dispersion attraction between  $\pi$ -orbitals in the phenyl groups in the ACSTA layers and  $\pi$ -electrons in the aromatic ring of the organic molecule. However, the role of the forming intermolecular H-bonds between the O-containing functional groups of ACSTA and the H-atoms of the  $-\text{COOH}$  group and the alkyl residues in the IBU molecule is significant. The interactions discussed are schematically represented in Fig. 9.

The conclusions drawn in the present study correspond to the observations of other scientists investigating the role of various non-covalent interactions working in tandem to provide multiple non-covalent intermolecular forces between drugs and carriers in view of the adsorption of non-steroidal anti-inflammatory pharmaceuticals on different types of activated carbons and subsequent *in vitro* release of the target compounds.<sup>37,40–43</sup>

Besides, IBU belongs to the BCS class II drugs, which characterize with low solubility, high permeability, and bioavailability limited by their solvation rate. Thus, the establishment of a correlation between the fundamental parameters: *in vivo* bioavailability and the *in vitro* solvation of IBU, is essential

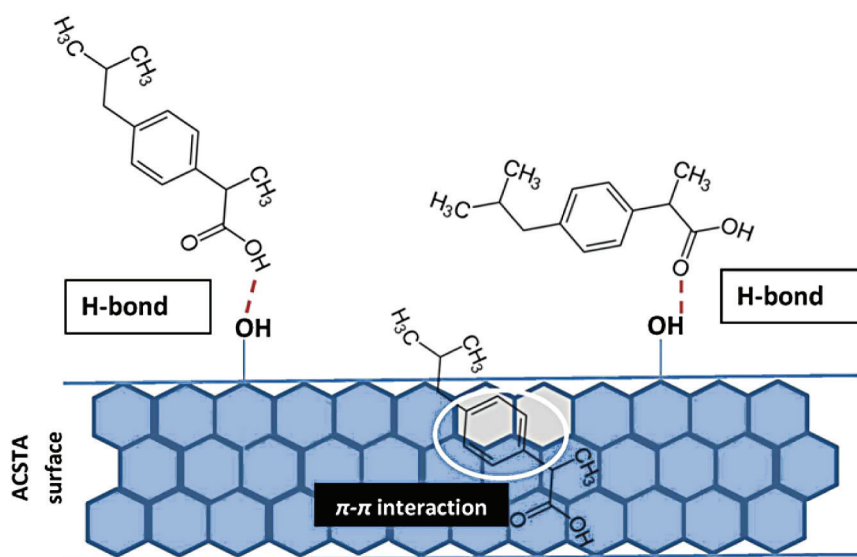


Fig. 9 – Physicochemical interaction between ACSTA surface functional groups and IBU molecules

for defining the oral drug absorption in humans, their pharmacokinetics, pharmacodynamics pathways in the body, and the therapeutic efficiency of newly designed drug-carrier microformulations.<sup>41,44</sup>

## Conclusions

The FTIR analyses provided evidence of the high extent of IBU encapsulation in the prepared NSAID/carbon carrier system, as the strong bands assigned to the vibration of the drug molecules were predominant. The highest achieved ACSTA encapsulation efficiency towards IBU at equilibrium conditions was  $E = 52\%$ , and the maximum equilibrium capacity  $q_e^{\max} = 19.5 \mu\text{g IBU mg}^{-1}$  ACSTA. The four-parameter Baudu model presented the best description of the encapsulation behavior of the NSAID on the activated carbon. The significant consistency of the mixed surface reaction and diffusion controlled kinetics model outlined the rate-limiting role of diffusion during the initial 58 min of the drug microencapsulation, followed by adsorption of the biologically active molecules on the active sites through a surface reaction mechanism. The value of Biot number  $Bi > 100$  defined the process of IBU encapsulation on ACSTA microparticles as controlled predominantly by intraparticle solid phase diffusion. The significant applicability of the semi-empirical Korsmeyer-Peppas model demonstrates the complex influence of probable abrasion of the solid microcarrier due to mechanical scraping of the surface and diffusion on the *in vitro* IBU release of IBU during the initial stages combined with the limiting role of Fickian diffusion mechanism during the later stages of the release process. The predominant host-guest interactions between IBU molecules and the carrier include hydrophobic  $\pi$ - $\pi$  interactions and intermolecular H-bonds between ACSTA O-containing functional groups and the H-carboxylic atoms and alkyl residues in the IBU molecule. The applicability of ACSTA microparticles as appropriate NSAID carriers in pharmacy and medicine was proven by the minimum ash content of the matrix, as well as the achieved prolonged and efficient *in vitro* drug release, consistent with the single dosage prescriptions and recommended dosage allowances for humans. To study in details the probable variations of the newly designed drug-carrier system behavior in real biological environment, future microbiological and clinical experiments shall be conducted.

## ACKNOWLEDGEMENTS

The study was supported financially by Scientific Project No. 04/16 VMF, Trakia University, Stara Zagora, Bulgaria.

## References

- Garrido-Herrera, F. J., Gonzalez-Pradas, E., Fernandez-Pérez, M., Controlled release of isoproturon, imidacloprid, and cyromazine from alginate-bentonite-activated carbon formulations, *J. Agric. Food. Chem.* **54**(26) (2006) 10053.  
doi: <https://doi.org/10.1021/jf062084m>
- Gupta, A. K., Dey, B. K., Microencapsulation for controlled drug delivery: A comprehensive review, *Sunsari Tech. Coll. J.* **1**(1) (2012).  
doi: <https://doi.org/10.3126/stcj.v1i1.8660>
- Ahuja, G., Pathak, K., Porous carriers for controlled/modulated drug delivery, *Ind. J. Pharm. Sci.* **71**(6) (2009) 599.  
doi: <https://doi.org/10.4103/0250-474X.59540>
- Azaïs, Th., Tourné-Péteilh, C., Aussenac, F., Baccile, N., Coelho, C., Devoisselle, J., Babonneau, F., Solid-state NMR study of ibuprofen confined in MCM-41 material, *Chem. Mater. J.* **18**(26) (2006) 6382.  
doi: <https://doi.org/10.1021/cm061551c>
- Baláu, L. E., Aelenei, N., Papa, M. I., Preparation and characterization of sodium alginate-chitosan microparticles for controlled release of ibuprofen in a sustainable way, *Environ. Eng. Manag. J.* **8**(3) (2009) 559.  
doi: <http://doi.org/10.30638/eemj.2009.077>
- Huei, G. O. S., Muniyandy, S., Sathasivam, T., Veeramachineni, A. K., Janarthanan, P., Iron cross-linked carboxymethyl cellulose-gelatin complex coacervate beads for sustained drug delivery, *Chemical Papers* **70**(2) 2016 243.  
doi: <https://doi.org/10.1515/chempap-2015-0197>
- Ghaheh, F. S., Alihosseini, A. K. F., Gomes, A., Ribeiro, A., Cavaco-Paulo, A., Silva, C., Protein-based nanoformulations for  $\alpha$ -tocopherol encapsulation, *Eng. Life Sci.* **17** (2017) 523.  
doi: <https://doi.org/10.1002/elsc.201600188>
- Oh, A., Yun, J., Kim, H., Controlled release behavior of PCL/PEO/activated carbon composite microcapsule, *J. Polym. Res.* **18** (2011) 2441.  
doi: <https://doi.org/10.1007/s10965-011-9658-7>
- McCary, S. E., Rybolt, T. R., Storage and timed release of acetaminophen from porous carbonaceous materials, *Open J Phys Chem.* **3** (2013) 76.  
doi: <https://doi.org/10.4236/ojpc.2013.32010>
- Fernández-Pérez, M., Villafranca-Sánchez, M., Flores-Céspedes, F., Garrido-Herrera, F. J., Pérez-García, S., Use of bentonite and activated carbon in controlled release formulations of carbofuran, *J. Agric. Food Chem.* **53**(17) (2005) 6697.  
doi: <https://doi.org/10.1021/jf051342x>
- Roivas, L., Neuvonen, P. J., Drug adsorption onto activated charcoal as a means of formulation, *Methods Find. Exp. Clin. Pharmacol.* **16**(5) (1994) 367.
- Nakamura, T., Kawasaki, N., Matsumoto, K., Tanada, S., Effect of particle size on the adsorption of theophylline onto activated charcoal, *in vitro* study, *Chudoku Kenkyu* **16**(1) (2003) 57.
- Tominaga, K., Sato, Sh., Hayashi, M., Activated charcoal as an effective treatment for bacterial vaginosis, *Pers. Med. Univ.* **1** (2012) 54.  
doi: <https://doi.org/10.1016/j.pmu.2012.05.009>
- Senthil Kumar, P., Ramalingam, S., Senthamarai, C., Niranjana, M., Vijayalakshmi, P., Sivanesan, S., Adsorption of dye from aqueous solution by cashew nut shell: Studies on equilibrium isotherm, kinetics and thermodynamics of interactions, *Desalination* **261**(1-2) 2010 52.  
doi: <https://doi.org/10.1016/j.desal.2010.05.032>

15. Dotto, G., Vieira, M., Esquerdo, V., Pinto, L., Equilibrium and thermodynamics of azo dyes biosorption onto *Spirulina platensis*, *Braz. J. Chem. Eng.* **30**(01) (2013) 13. doi: <https://doi.org/10.1590/S0104-66322013000100003>
16. Sivarajasekar, M., Baskar, R., Adsorption of Basic Magenta II onto H<sub>2</sub>SO<sub>4</sub> activated immature *Gossypium hirsutum* seeds: Kinetics, isotherms, mass transfer, thermodynamics and process design, *Arab. J. Chem.* **2014**(1) (2014). doi: <https://doi.org/10.1016/j.arabjc.2014.10.040>
17. Yaneva, Z., Staleva, M., Georgieva, N., Study on the host-guest interactions during caffeine encapsulation into zeolite, *Eur. J. Chem.* **6**(2) (2015) 169. doi: <https://doi.org/10.5155/eurjchem.6.2.169-173.1228>
18. Fenoglio, I., Fubini, B., Ghibaudi, E. M., Turci, F., Multiple aspects of the interaction of biomacromolecules with inorganic surfaces, *Adv. Drug. Deliv. Rev.* **63** (2011) 1186. doi: <https://doi.org/10.1016/j.addr.2011.08.001>
19. Gran, G., Determination of the equivalence point in potentiometric titrations—Part II. *Analyst* **77** (1952) 661.
20. Gran, G., Johansson, A., Johansson, S., Automatic titration by stepwise addition of equal volumes of titrant, Part VII. Potentiometric precipitation titrations, *Analyst* **106** (1981) 1109.
21. Ivanova, D., Kadukova, J., Kavulicova, J., Horvathova, H., Determination of the functional groups in algae *Parachlorella kessleri* by potentiometric titrations, *Nova Biotechnol. Chim.* **11**(2) (2012) 93. doi: <https://doi.org/10.2478/v10296-012-0010-3>
22. Moreno-Castilla, M., Lopez-Ramon, V., Carrasco-Marin, F., Changes in surface chemistry of activated carbons by wet oxidation, *Carbon* **38** (2000) 1995. doi: [https://doi.org/10.1016/S0008-6223\(00\)00048-8](https://doi.org/10.1016/S0008-6223(00)00048-8)
23. Shafeeyan, M. S., Wan, W. M. A. W., Houshmand, A., Shamiri, A., A review on surface modification of activated carbon for carbon dioxide adsorption, *J. Anal. Appl. Pyrolysis* **89** (2010) 143. doi: <https://doi.org/10.1016/j.jaap.2010.07.006>
24. Vuema, M. L., Pina, M. E., Batista de Carvalho, L. A. E., Conformational stability of ibuprofen: Assessed by DFT calculations and optical vibrational spectroscopy, *J. Pharm. Sci.* **97** (2008) 845. doi: <https://doi.org/10.1002/jps.21007>
25. Mopoung, S., Moonsri, Ph., Pallas, W., Khumpai, S., Characterization and properties of activated carbon prepared from Tamarind seeds by KOH activation for Fe(III) adsorption from aqueous solution, *Sci. World J.* **2015** (2015) 1. doi: <https://doi.org/10.1155/2015/415961>
26. Selvaraju, G., Kartini, N., Bakar, A., Production of a new industrially viable green-activated carbon from *Artocarpus integer* fruit processing waste and evaluation of its chemical, morphological and adsorption properties, *J. Clean. Prod.* **141** (2017) 989. doi: <https://doi.org/10.1016/j.jclepro.2016.09.056>
27. Trofymchuk, I. M., Roik, N., Belyakova, L., Sol-gel synthesis of ordered  $\beta$ -cyclodextrin-containing silicas, *Nanoscale Res. Lett.* **11** (2016) 174. doi: <https://doi.org/10.1186/s11671-016-1380-2>
28. Georgieva, N., Yaneva, Z., Comparative evaluation of natural and acid-modified layered mineral materials as rimifon-carriers using UV/VIS, FTIR, and equilibrium sorption study, *Cogent Chem.* **1**(1) (2015) 1. doi: <https://doi.org/10.1080/23312009.2015.1069723>
29. Yaneva, Z. L., Georgieva, N. V., Bekirska, L. L., Lavrova, S., Drug mass transfer mechanism, thermodynamics, and *in vitro* release kinetics of antioxidant-encapsulated zeolite microparticles as a drug carrier system, *Chem. Biochem. Eng. Q.* **32**(3) (2018) 281. doi: <https://doi.org/10.15255/CABEQ.2018.1319>
30. Tan, K. L., Hameed, B. H., Insight into the adsorption kinetics models for the removal of contaminants from aqueous solutions, *J. Taiwan Inst. Chem. E.* **74** (2017) 25. doi: <https://doi.org/10.1016/j.jtice.2017.01.024>
31. Wu, Sh., Zhao, X., Li, Y., Du, Q., Sun, J., Wang, Y., Wang, X., Xia, Y., Wang, Z., Xia, L., Adsorption properties of doxorubicin hydrochloride onto graphene oxide: Equilibrium, kinetic and thermodynamic studies, *Materials* **6** (2013) 2026. doi: <https://doi.org/10.3390/ma6052026>
32. Sugunalakshmi, M., Bava Bakrudeen, H., Abilash, B., Krishnan, P. N., Mandal, B., Inorganic clay mineral, montmorillonite for the adsorption of isoniazid drug, formulations and release studies, *Int. J. Rec. Adv. Eng. Technol. (IJRAET)* **2**(9) (2014) 2347.
33. Bany-Aiesh, H., Banat, R., Al-Souod, K., Kinetics and adsorption isotherm of ibuprofen onto grafted  $\beta$ -CD/chitosan polymer, *Am. J. Appl. Sci.* **12**(12) (2015) 917. doi: <https://doi.org/10.3844/ajassp.2015.917.930>
34. Siami, F., Ahmadpanahi, H., Heidarinasab, A., Moniri, E., Akbarzadeh, A., Shahmabadi, H. E., Investigation of adsorption kinetic of doxorubicin onto iron oxide magnetic nanoparticles functionalized with poly(acrylic acid)/allyl alcohol, *Int. J. Med. Res. Health Sci.* **5**(9S) (2016) 188.
35. Yaneva, Z., Georgieva, N., Chapter 5. Physicochemical and morphological characterization of pharmaceutical nanocarriers and mathematical modeling of drug encapsulation/release mass transfer processes, Book: *Nanoscale Fabrication, Optimization, Scale-up and Biological Aspects of Pharmaceutical Nanotechnology*, 1st Ed., 2017, Editor: Alexandru Grumezescu, © William Andrew 2018, Elsevier. Paperback ISBN: 9780128136294.
36. Chang, E. E., Wan, J., Kim, H., Liang, C., Dai, Y., Chiang, P., Adsorption of selected pharmaceutical compounds onto activated carbon in dilute aqueous solutions exemplified by acetaminophen, diclofenac, and sulfamethoxazole, *Sci. World J.* **2015** (2015) 1. doi: <https://doi.org/10.1155/2015/186501>
37. Bushra, R., Aslam, N., An overview of clinical pharmacology of ibuprofen, *Oman Med. J.* **25**(3) (2010) 155.
38. Peppas, N. A., Sahlin, J. J., A simple equation for the description of solute release. III. Coupling of diffusion and relaxation, *Int. J. Pharm.* **57** (1989) 169. doi: [https://doi.org/10.1016/0378-5173\(89\)90306-2](https://doi.org/10.1016/0378-5173(89)90306-2)
39. Pawlish, G., Spivack, K., Gabriel, A., Huang, Z., Comolli, N., Chemotherapeutic loading via tailoring of drug-carrier interactions in poly (sialic acid) micelles, *AIMS Bioeng.* **5**(2) (2018) 106. doi: <https://doi.org/10.3934/bioeng.2018.2.106>
40. Bahamon, D., Carro, L., Guri, S., Vega, L. F., Computational study of ibuprofen removal from water by adsorption in realistic activated carbons, *J. Colloid Interface Sci.* **498** (2017) 323. doi: <https://doi.org/10.1016/j.jcis.2017.03.068>
41. Rahma, A., Munir, M. M., Khairurrijal, Prasetyo, A., Suen-do, V., Rachmawati, H., Intermolecular interactions and the release pattern of electrospun curcumin-polyvinylpyrrolidone fiber, *Biol. Pharm. Bull.* **39**(2) (2016) 163. doi: <https://doi.org/10.1248/bpb.b15-00391>
42. Hao, Y. M., Li, K., Entrapment and release difference resulting from hydrogen bonding interactions in noisome, *Int. J. Pharm.* **403** (2011) 245. doi: <https://doi.org/10.1016/j.ijpharm.2010.10.027>

43. Ryabenkova, Y., Jadav, N., Conte, M., Hippler, M. F., Reeves-McLaren, N., Coates, P. D., Twigg, P., Paradkar, A., Mechanism of hydrogen-bonded complex formation between ibuprofen and nanocrystalline hydroxyapatite, *Langmuir* **33**(12) (2017) 2965.  
doi: <https://doi.org/10.1021/acs.langmuir.6b04510>
44. Salem, N. A., Yakoot, S. M., Non-steroidal anti-inflammatory drug ibuprofen adsorption using rice straw based biochar, *Int. J. Pharmacol.* **12**(7) (2016) 729.  
doi: <https://scialert.net/abstract/?doi=ijp.2016.729.736>
45. Belhamdi, B., Merzougui, Z., Trari, M., Addouna, A., A kinetic, equilibrium and thermodynamic study of l-phenylalanine adsorption using activated carbon based on agricultural waste (date stones), *J. Appl. Res. Technol.* **14** (2016) 354.  
doi: <https://doi.org/10.1016/j.jart.2016.08.004>
46. Amidon, G. L., Lennernäs, H., Shah, V. P., Crison, J. R., A theoretical basis for a biopharmaceutic drug classification: The correlation of *in vitro* drug product dissolution and *in vivo* bioavailability, *Pharm Res.* **12**(3) (1995) 413.  
doi: <https://doi.org/10.1023/A:1016212804288>